AGU PUBLICATIONS

Geophysical Research Letters

RESEARCH LETTER
10.1002/2016GL072008

Key Points:
- Identification of bathymetric/morphologic contrasts along and between different hotspot tracks
- Scaling formulation for mantle plume lithosphere interaction and bathymetry production
- Support on observational data of global scope

Supporting Information:
- Supporting Information S1

Correspondence to:
F. Orellana-Rovirosa,
f_orellana@berkeley.edu

Citation:
Orellana-Rovirosa, F., and M. Richards (2017), Rough versus smooth topography along oceanic hotspot tracks: Observations and scaling analysis, *Geophys. Res. Lett.*, *44*, 4074–4081, doi:10.1002/2016GL072008.

Received 19 NOV 2016
Accepted 22 FEB 2017
Accepted article online 26 FEB 2017
Published online 13 MAY 2017

Rough versus smooth topography along oceanic hotspot tracks: Observations and scaling analysis

Felipe Orellana-Rovirosa[1] and Mark Richards[1]

[1]Department of Earth and Planetary Science, University of California, Berkeley, California, USA

Abstract Some hotspot tracks are topographically smooth and broad (Nazca, Carnegie/Cocos/Galápagos, Walvis, Iceland), while others are rough and discontinuous (Easter/Sala y Gomez, Tristan-Gough, Louisville, St. Helena, Hawaiian-Emperor). Smooth topography occurs when the lithospheric age at emplacement is young, favoring intrusive magmatism, whereas rough topography is due to isolated volcanic edifices constructed on older/thicker lithosphere. The main controls on the balance of intrusive versus extrusive magmatism are expected to be the hotspot swell volume flux Q_s, plate hotspot relative speed v, and lithospheric elastic thickness T_e, which can be combined as a dimensionless parameter $R = (Q_s/v)^{1/2}/T_e$, which represents the ratio of plume heat to the lithospheric heat capacity. Observational constraints show that, except for the Ninetyeast Ridge, R is a good predictor of topographic character: for $R < 1.5$ hotspot tracks are topographically rough and dominated by volcanic edifices, whereas for $R > 3$ they are smooth and dominated by intrusion.

1. Introduction

Many oceanic hotspot track segments can be characterized in terms of smooth or rough topography, likely reflecting the relative roles of intrusive versus extrusive magmatism (absence or dominance of volcanic edifices). The two conspicuous examples that motivated this study are noticeable transitions from rough to smooth topography along the Easter Island hotspot track (rough Easter/Sala y Gomez chains versus broad and smooth Nazca Ridge segment), and the Tristan da Cunha hotspot track (rough Tristan/Gough chains versus relatively smooth Walvis Ridge segment) (see Figures 1a and 1b). Smooth topography examples, with across-axis widths ≥120 km, include the Rio Grande Rise, the Carnegie/Cocos/Galápagos system, Iceland, the Tuamotu Ridge, Broken Ridge, and various segments along the Ninetyeast Ridge/Kerguelen and Réunion/Chagos/Lacadive track. Gravity studies show that these systems are currently in near-Airy isostatic equilibrium [*Dingle and Simpson*, 1977; *Couch and Whitsett*, 1981; *Pilger and Handshumacher*, 1981; *Watts*, 2001; *Hampel et al*., 2004], and plate tectonic reconstructions show that the lithospheric age of emplacement was young; hence, the overlying plate was thermally thin and rheologically weak, consistent with petrological models for the role of intrusion along young oceanic hotspot tracks [*Richards et al*., 2013].

In contrast, other hotspot tracks are relatively rough and discontinuous, dominated by islands and seamounts with horizontal widths ≤60 km. Besides the Easter/Sala y Gomez and Tristan/Gough chains, examples include the Louisville chain, St. Helena track, Juan Fernandez Ridge, and most of the Hawaiian-Emperor chain, among many others. These systems were formed on old and thick oceanic lithosphere [*Pilger and Handshumacher*, 1981; *Calmant et al*., 1990; *Lyons et al*., 2000; *Hieronymus and Bercovici*, 2001; *Watts*, 2001; *Hillier*, 2007; *Contreras-Reyes et al*., 2010] with significant elastic lithospheric strength at the time of emplacement.

These distinct styles of topographic/bathymetric expression among different hotspot tracks present an opportunity to better understand the underlying processes controlling hotspot activity. In particular, the abrupt transitions along the two systems illustrated in Figure 1 suggest a relatively simple geodynamic explanation in terms of just a few key parameters.

2. A Simple Scaling Relation

We hypothesize that smooth hotspot topography occurs when the overlying lithosphere is weak and thin (young), unable to support large volcanic complexes [*Feighner and Richards*, 1994], thus allowing for broadly intrusive magmatism in the lower crust to dominate over extrusion [*Richards et al*., 2013; *Orellana-Rovirosa and Richards*, 2015]. Accordingly, smooth topography should occur when the thermal energy available

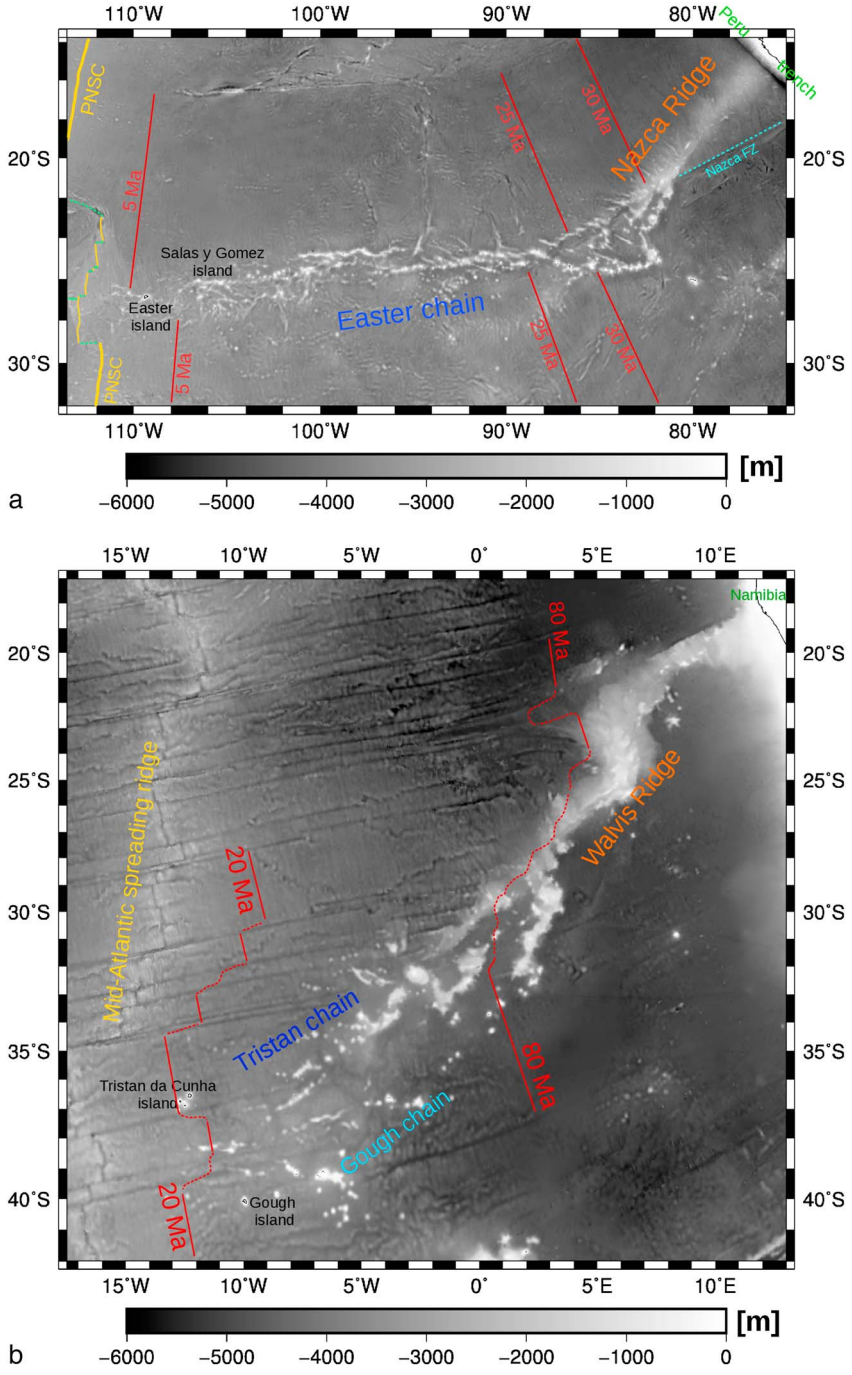

Figure 1. (a) Topographic map of the Nazca-Easter hotspot track region. Volcanically active Easter Island and Sala y Gomez chain marks the most recent activity of the Easter hotspot beneath lithosphere of age >7 Ma (Figure 2). Extending eastward ~2500 km, this initially rough hotspot track exhibits horizontal length scales <40 km. It transitions to the Nazca Ridge, emplaced on very young lithosphere [*Pilger and Handshumacher*, 1981], and characterized by a smooth, elevated topographic rise >200 km wide (due to thickened crust but absent large volcanic edifices, Figure 2), extending another 1000 km northeastward before encountering the Peruvian subduction zone. PNSC stands for Pacific-Nazca spreading center, also known as the East Pacific Rise. (b) Topographic map of the Walvis-Tristan-Gough hotspot track region. The broad and smooth Walvis Ridge, off the west coast of Africa, formed as an "near/on-ridge" system starting ~130 Ma ago and is characterized by a smooth, elevated topographic rise ~330 km wide. At about 80 Ma, the westward moving Mid-Atlantic (spreading) Ridge left (after crossing over) the Tristan hotpot [*Kumar*, 1979; *O'Connor and Duncan*, 1990; *Sleep*, 2002], the latter producing rough hotspot track topography characterized by islands and seamounts with horizontal length scales <70 km. The Tristan plume is currently active beneath lithosphere of age ~22 Ma.

from the plume is sufficient to thin the lithosphere as it passes over the plume. To estimate the ratio of available plume heat to lithospheric heat capacity, we consider a strip of hot, buoyant plume material (as in *Sleep* [1996]) of thickness s beneath a plate of thickness T_e that is moving at relative speed v, generating a topographic swell of width L (perpendicular to the motion of the plate) and average height h. Assuming that isostatic balance holds roughly at the horizontal length scale of the swell, we have

$$s\cdot\left(\rho_m-\rho_p\right)\cdot g = h\cdot(\rho_m-\rho_w)\cdot g \tag{1}$$

where g is the acceleration of gravity, and the densities ρ_m, ρ_p, and ρ_w are, respectively, those of the mantle, the hot plume material, and water (assuming submerged topography). Multiplying by the swell width L and plate velocity v, assuming that the mantle plume density difference is due to the average excess plume temperature $\theta_p-\theta_m$ with thermal expansivity α_v, we obtain

$$s\cdot L\cdot v\cdot\rho_m\cdot\alpha_v\cdot\left(\theta_p-\theta_m\right) = h\cdot L\cdot v\cdot(\rho_m-\rho_w) \tag{2}$$

$$\text{or } s\cdot L\cdot v\cdot\rho_m\cdot C_p\cdot\left(\theta_p-\theta_m\right) = \left(C_p/\alpha_v\right)\cdot h\cdot L\cdot v\cdot(\rho_m-\rho_w) \tag{3}$$

where the heat capacity is C_p. The left side of this equation is just the plume excess heat flux, thus

$$\dot{U}_P = \left(C_p/\alpha_v\right)\cdot h\cdot L\cdot v\cdot(\rho_m-\rho_w) \tag{4}$$

Defining $\dot{U}_L$ as the thermal energy rate necessary to raise the overlying lithospheric mantle temperature to that of the underlying mantle, θ_m (at the base of the elastic lithosphere), and approximating a roughly linear geotherm with θ_M right at the Moho (and uppermost mantle), we obtain the rate of heating necessary to effectively "remove" the overlying lithosphere

$$\dot{U}_L = L\cdot T_e\cdot v\cdot\rho_m\cdot C_p\cdot(\theta_m-\theta_M)/2 \tag{5}$$

$$\text{or } \dot{U}_L = L\cdot T_e\cdot v\cdot\left(C_p/\alpha_v\right)\cdot(\rho_M-\rho_m)/2(\text{after multiplying through by } \alpha_v/\alpha_v) \tag{6}$$

where ρ_M, ρ_m are reference temperature-dependent densities of the lithospheric mantle (at the corresponding temperatures). We now form the heat flux ratio

$$R_0 = \dot{U}_p/\dot{U}_L = (h/T_e)\cdot 2\cdot(\rho_m-\rho_w)/(\rho_m-\rho_M) \tag{7}$$

We expect that when R_0 is large (>1), the lithosphere will be thermally reset by the plume, resulting in a larger fraction of magmatic intrusion into the crust, and hence relatively smooth topography.

Unfortunately, the scarcity of published estimates of hotspot swell heights h (aside from *King and Adam* [2014]) renders the above formula somewhat impractical. Therefore, we instead consider a closely related scaling formulation: Recognizing the swell volume flux $Q_s = L\cdot h\cdot v$ as the surface expression of the plume buoyancy, we consider the alternative dimensionless ratio:

$$R = \sqrt{(Q_s/v)}/T_e \tag{8}$$

(We noted at the outset that Q_s, v, and T_e would likely be the main controlling independent variables for any particular hotspot track, so that they could likely be combined into a dimensionless group sufficient to characterize the observations). The numerator of this function is the geometric-mean linear dimension of the swell cross section. Statistical analysis of the hotspot swell data compiled by *King and Adam* [2014], as well as some theoretical considerations, suggest the function $(Q_s/v)^{1/2} = (L\cdot h)^{1/2}$ is approximately proportional to h, the average swell height. Thus, the dimensionless parameters R_0 and R are both approximately proportional to h/T_e, and hence to each other, so that both characterize the ability of the plume to thermally erode the overlying lithosphere and may suffice to predict a plume's topographic expression. Because estimates for Q_s, v, and T_e have been compiled for hotspot tracks by numerous authors (Figure 2), we examine how smoothness and roughness are correlated with estimated values of R along different oceanic hotspot tracks.

3. Results

Figure 2 contains data on hotspot tracks for which the parameters in the scaling relation for R are sufficiently constrained in the literature and uses various symbols to indicate the character of topography—smooth

	age [Ma]	Qs [m3/s]	v [cm/yr]	Te [km]	LAE [Ma]	R	+-R Error	Bathymetry	HTL [km]
Nazca	43	0.42 ?	7.39	3.5 ?	0 ?	**3.83**	-1.5 , +2.0	S	200-240
Nazca	35	0.42	7.39	3.5	0	**3.83**	-0.7 , +1.0	S	100-200
Trans	26.5	0.42	8.32	3.5	0	**3.61**	-0.5 , +0.6	T	30-150
Easter	15	0.84	9.25	6.2	3.04	**2.73**	-0.4 , +0.4	R	< 40
Easter	0	0.84	9.25	9.4	7.0	**1.80**	-0.3 , +0.3	R	< 35
Walvis	130	0.531 ?	2.8	7.5 ?	0 ?	**3.26**	-1.5 , +2.0	S	200-250
Walvis	100	0.531	2.8	7.5	0	**3.26**	-1.0 , +1.3	S	200-270
Trans	80	0.531	2.62	7.5	0	**3.37**	-0.6 , +0.8	STR	50-190
Tristan-Gough	40	0.332	2.44	11.6	10.8	**1.79**	-0.4 , +0.5	R	30-70
Tristan-Gough	0	0.390	2.44	16.45	21.5	**1.37**	-0.3 , +0.4	R	10-30
Louisville	60	0.698	4.5	22.5	40	**0.98**	-0.4 , +0.5	R	< 50
Louisville	35	0.698	7.4	26.3	55	**0.66**	-0.3 , +0.4	R	< 60
Louisville	12.5	0.698	6.4	24.5	47.5	**0.76**	-0.2 , +0.3	R	< 35
Louisville	0	0.698	6.4	19.4	30	**0.96**	-0.2 , +0.3	R	< 10
Carnegie	15	0.11 ?	3	4.5	0	**2.39**	-1.5 , +2.0	ST	50-100
Galapagos	5	0.33	3.7	5	2	**3.36**	-0.6 , +1.0	S	120-180
Galapagos	0	0.33	3.7	11.8	11	**1.42**	-0.3 , +0.5	T	50-100
Iceland	9	0.32 ?	0.5 ?	4.5 ?	0 ?	**9.99**	-4.0 , +10.0	S	400-470
Iceland	0	0.64	0.5 ?	15.9	20	**4.00**	-1.5 , +6.0	S	400-470
Hawaii	47	1	6.27	31.8	80	**0.71**	-0.3 , +0.3	R	20-50
Hawaii	30	2.5	6.27	32.3	82.9	**1.10**	-0.2 , +0.2	R	15-80
Hawaii	15	7.5	9.2	32.8	85.4	**1.55**	-0.2 , +0.2	T	120-160
Hawaii	8	4.2	9.2	33.03	86.6	**1.15**	-0.1 , +0.2	R	40-90
Hawaii	2	12.5	9.2	33.2	87.6	**1.97**	-0.1 , +0.2	T	160-200
Hawaii	0	3.02	9.2	33.3	88	**0.97**	-0.1 , +0.2	RT	100-140
Ninetyeast	77	0.18 ?	10	7.9	5	**0.95**	-0.5 , +2.0	ST	160-250
Ninetyeast	73	0.18 ?	10	5	0	**1.51**	-0.5 , +2.0	ST	200-300
Ninetyeast	62	0.18 ?	12	5	0	**1.38**	-0.5 , +1.5	ST	100-150
Ninetyeast	55	0.18 ?	12	5	0	**1.38**	-0.5 , +1.0	ST	140-240
Ninetyeast	45	0.18 ?	7	13.7	15	**0.66**	-0.5 , +1.0	ST	140-240
St. Helena	50	0.16	2.2	16.80	22.5	**0.90**	-0.8 , +1.0	R	10-40
St. Helena	20	0.27	2.15	20.19	32.5	**0.99**	-0.6 , +0.8	R	10-50
St. Helena	0	0.13	2.1	20.95	35	**0.67**	-0.3 , +0.4	R	< 40
Reunion	40	0.233 ?	3.4 ?	4	0	**3.67**	-1.5 , +2.0	S	170-280
Reunion	30	0.465	2.8	14.8	17.5	**1.55**	-0.5 , +0.8	ST	100-200
Reunion	20	0.465	2.5	23.8	45	**1.02**	-0.4 , +0.6	T	80-180
Reunion	0	0.465	1.9	27.4	60	**1.01**	-0.3 , +0.4	T	90-150

Figure 2. Summary information for the hotspot tracks with sufficient published constraints: Left to right, hotspot track age (Ma), swell volume flux Q_s (m^3/s), plate hotspot horizontal relative speed v (cm/yr), lithospheric elastic thickness T_e (km), lithospheric age at emplacement LAE (Ma), nondimensional function R, approximate error estimates on R, qualitative topographic style assessment (coded as in Figure 3), characteristic horizontal (transverse) topographic length scale HTL (km). Away from spreading centers, T_e was computed using the age-dependent thickness defined by the 450°C isotherm, following *Watts* [1978]. Corresponding published values of T_e were used at spreading centers. For the swell volume fluxes Q_s, a factor of 1/2 is applied for on-ridge systems. Exceptions are Walvis ridge where the on-ridge value at 80 Ma is taken from *Adam et al.* [2007] and Galápagos where a tentative 1/3 factor was used when the hotspot was located mainly on the Cocos plate side.

(orange circles), rough (blue diamonds), and transitional (brown squares). R is computed for topographically coherent segments along individual hotspot tracks. Figure 3 plots these estimates of R versus the estimated lithospheric age at emplacement (LAE). Figures 2 and 3 show a largely consistent relation between R and topographic character: for $R < 1.5$ topography tends to be rough, for $1.5 < R < 3$ topography is transitional, and for $R > 3$ topography tends to be smooth, consistent with the energy ratio hypothesis contained in the formulations for R_0 and R in the previous section. Exceptions to these trends are treated in the discussion section.

The results of Figure 3 show some scatter in the relation between bathymetric character and R, which is not unexpected given uncertainties in the underlying data. Additionally, magma emplacement mode (intrusion versus extrusion) may also depend upon other lithospheric properties not captured by R, since lithospheric properties are not solely dependent upon age or elastic/thermal thickness. For example, effective

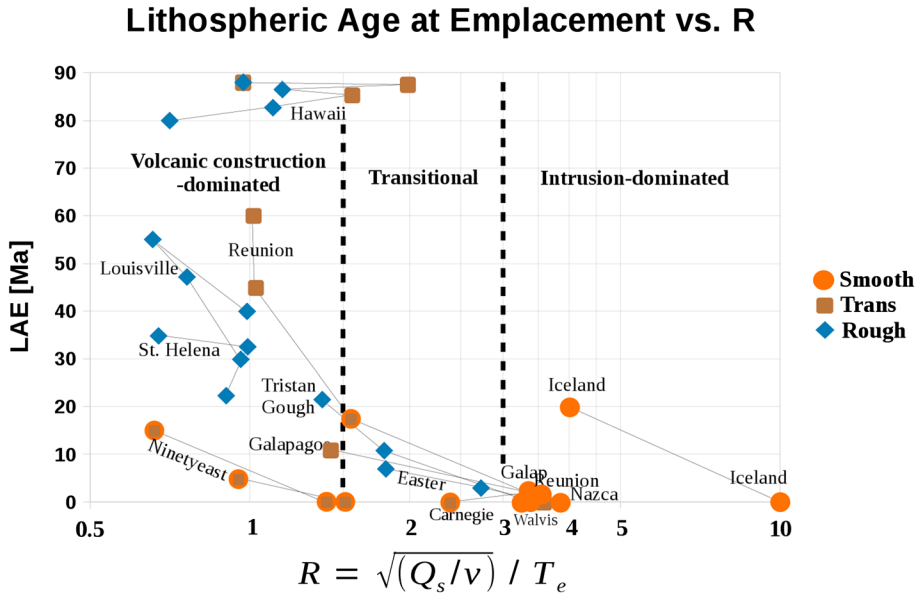

Figure 3. Lithospheric age at time of magma emplacement LAE (Ma) versus the dimensionless heat flux ratio *R*, from data in Figure 2. Symbols indicate the topographic style. Away from spreading centers, the lithospheric elastic thickness $T_e \sim (\mathrm{LAE})^{1/2}$. The Hawaiian plume appears as an outlier due to a much older LAE and a very high buoyancy flux. There is an overall trend: The systems become smoother as *R* increases.

lithospheric permeability to melt transport (e.g., via fractures and diking) is poorly understood and may depend upon the state of stress. Episodes of plate motion reorganization likely cause abrupt stress field changes, and hence changes in fracture density. Pacific-Nazca plate motion reorganization between 30 and 25 Ma [*Pilger and Handshumacher*, 1981], which caused only a slight bend in the Hawaiian and Louisville ridges [*Lonsdale*, 1988; *Wessel and Kroenke*, 2009], appears to have coincided with a dramatic change in the Nazca-Easter system, wherein several branches of elongated bathymetry may be the result of lithospheric fractures (such as the one aligned with the Nazca fracture zone; see Figure 1a).

Figure 2 also lists a measure of the characteristic range of horizontal length scales for each hotspot track segment, labeled the horizontal topographic length scale (HTL). These HTL ranges represent systematic estimates of the horizontal linear dimension of the characteristic topographic features, taken in the across-track direction for smooth (continuous) tracks and in any direction for isolated volcanic edifices (rough tracks). Figure 4 indicates the expected tendency for HTL to increase as the heat flux ratio *R* increases. This relation also implies topological changes: At low *R* values the seamounts are small, isolated, and disconnected from each other; as *R* increases they are broader and more frequent (more closely spaced) leading to increased connectivity (this connectivity of the bathymetric bumps also implies their overlapping). Above a threshold of $R \sim 3$, the topographic features are essentially broad platforms, with most magmatism being intrusive [*Feighner and Richards*, 1994; *Richards et al.*, 2013;

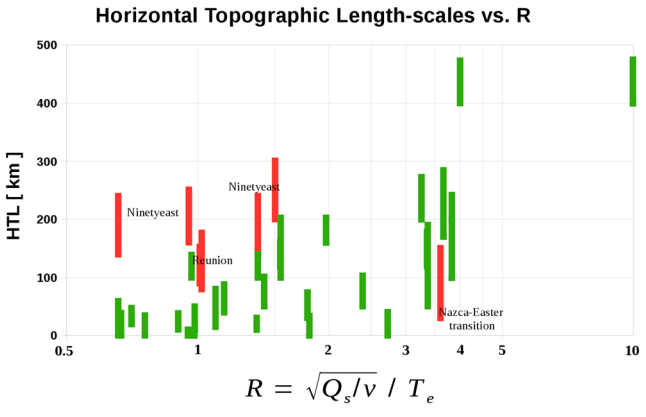

Figure 4. Horizontal topographic length scale HTL (km) versus the dimensionless heat flux ratio *R*. For each computed *R* value, a range in HTL (measured from Google Earth) is presented (Figure 2). The overall set of observations (green bars) shows the expected increase of HTL with *R*. Deviating from this trend (red bars) are the Ninetyeast Ridge and to some extent Reunion and the Nazca-Easter transition region (see text).

Orellana-Rovirosa and Richards, 2015]. Deviating from this trend (red bars) are the Ninetyeast Ridge (with HTL up to 300 km), and to some extent Reunion (with HTL up to 180 km) and the transition region along Nazca-Easter (HTL as low as 30 km), all of which were influenced by preexisting fracture zones (see section 4).

4. Discussion

The principal observations motivating this study are the conspicuous transitions from smooth to rough topography along the Easter and Tristan hotspot tracks (Figures 1a and 1b). These transitions are explainable in terms of very young (near-ridge) versus relatively mature (off-ridge) lithospheric emplacement environments. We have attempted to cast these observations into a larger context by examining other hotspot tracks where sufficient constraining data exist, and by developing a scaling parameter R_0, the ratio of available plume heat to lithospheric heat capacity. This scaling is directly related to the parameter R which largely captures the observed behavior in terms of the controlling variables Q_s, v and T_e. Using the dimensionless parameter R_0 (equation (7)) instead of R (equation (8)) would simply introduce a factor of ~4.9 in the scaling (a shift in the numerical R values for smooth versus rough topography). Using the estimated thermal lithospheric thickness (perhaps corresponding to the 1250°C isotherm) instead of the estimated elastic thickness T_e (corresponding to the 450°C isotherm) would, likewise, merely scale the R values by a constant factor of ~0.2, and the conversion factor from R to R_0 would become ~1.5. We find T_e preferable, because it can be compared with present-day estimates from gravity and bathymetry analysis.

For the scaling calculations we have performed, there is a transition from rough to smooth topography in the approximate range $1.5 < R < 3$ for most of the hotspot tracks examined, and this transition is generally gradual:

1. At 80 Ma, the Mid-Atlantic Ridge moved away from Tristan plume [*Nurnberg and Muller*, 1991] with a gradual bathymetric transition: the single-branched broad Walvis rise splits into two narrower (~90 km width) branches (Tristan and Gough) with visible individual seamounts. In this region R decreases from ~3.3 to ~2.0 (during 80–60 Ma).
2. During the period 8 to 1 Ma ago, the Hawaiian plume increased its buoyancy flux by a factor of ~3 [*Wessel*, 2016], while v and T_e did not change substantially. Correspondingly, in topographic expression, the ridge horizontal length scale increased from ~60 km to ~200 km, accompanied by a notable increase in continuity/connectivity. In this interval, R increases from ~1.2 to ~2.0.

The Ninetyeast Ridge deviates from the global trend (Figure 3), exhibiting transitional to smooth morphology at rather low values of R (<1.6). Spreading ridge jumps (perhaps controlled by the plume itself causing zones of weakness), as well as the apparently variable relative motion, v, between the Indian plate and the Kerguelen/Ninetyeast hotspot, cause the LAE values to vary in ways not well captured by the formulation used here. The lack of robust estimates for the Kerguelen plume buoyancy flux prior to 40 Ma makes the problem more challenging.

Moreover, we note that there is a pervasive N-S trending set of fracture zones parallel to the Ninetyeast hotspot track [*Sreejith and Krishna*, 2013, 2015], perhaps promoting "upstream" migration of plume material and magma from the mantle plume source through the fractures. This might weaken the lithosphere in advance of the principal large-scale magmatism (that typically occurs only above and downstream of the source), thus facilitating lithospheric deformation and intrusive magmatism, and potentially leading to smoother bathymetry.

The Reunion hotspot system deviates slightly from the expected trend, with transitional morphologies at rather low values of $R \sim 1$. This may be due to biased estimates of the Reunion plume buoyancy flux owing to the Mahanoro-Wilshaw and Mauritius fracture zones that bound the last ~30 Ma of hotspot track formation [*Torsvik et al*., 2013].

Some complexity arises when the moving spreading centers are in the close vicinity of mantle plumes: a fraction of the plume material may drain toward the spreading center and then diverge due to plate spreading, creating subordinated V-shaped axial tracks in addition to the principal hotspot track, as pointed out by *Sleep* [2002]. These tracks are evident in some cases, but otherwise, they tend to be merged with the rest of the

bathymetric signals especially on young lithosphere where massive intrusion and magmatism shapes the bathymetry.

Older hotspot-related volcanic edifices formed initially above sea level are subject to erosional flattening, which could skew the evaluation of topographic character to some degree for older hotspot tracks. For example, on Walvis Ridge (age >80 Ma) and northern Ninetyeast Ridge (age > 70 Ma) the bathymetric character was likely rougher back in time. Nevertheless, present-day near-ridge systems such as Iceland (or to some extent Galápagos) exhibit highly smooth topography. These systems have present-day LAE values >10 Ma, perhaps comparable to the near-ridge Walvis Ridge prior to ~100 Ma.

Although the scaling parameter $R(Q_s, v, T_e)$ is not a perfect predictor of the character of hotspot track topography or of the balance of intrusive to extrusive magmatism, it does account to first order for many of the global observations in Figure 2 in terms of the expected controlling variables. Some scatter in the results indicates additional complexity, such as lithospheric properties altered by stress and fracturing or other inherited lithospheric properties not captured simply by plate age and elastic thickness.

The formulation presented here emphasizes the recognition of the main controlling variables of the problem and its understanding from a functional perspective. The present study suggests a useful framework for future modeling studies of the development of hotspot track topography, especially in regard to the balance of intrusive versus extrusive processes during hotspot track emplacement.

Acknowledgments

The authors thank Sally Gibson, Eduardo Contreras-Reyes, Dennis Geist, Seth Saltiel, and Tushar Mittal for helpful suggestions on an earlier version of this manuscript, and Norm Sleep and Shijie Zhong for their constructive reviews. Consultation of details regarding the data and processes, when further beyond the references, should be directed to the first author at felipeorellanarovirosa@gmail.com. This work was supported by CONICYT Chile, the U.S. National Science Foundation, and the Esper Larsen Fund at UC Berkeley.

References

Adam, C., V. Vidal, and J. Escartín (2007), 80-Myr history of buoyancy and volcanic fluxes along the trails of the Walvis and St. Helena hotspots (S. Atlantic), *Earth Planet. Sci. Lett.*, *261*(3), 432–442.

Bjarnason, I. P. (2008), An Iceland hotspot saga, *Jökull*, *58*, 3–16.

Calmant, S., J. Francheteau, and A. Cazenave (1990), Elastic layer thickening with age of the oceanic lithosphere: A tool for prediction of the age of volcanoes or oceanic crust, *Geophys. J. Int.*, *100*, 59–67.

Cochran, J. R. (1979), An analysis of isostasy in the world's oceans: 2. Midocean ridge crests, *J. Geophys. Res.*, *84*, 4713–4729, doi:10.1029/JB084iB09p04713.

Coffin, M. F., M. S. Pringle, R. Duncan, T. P. Gladczenko, M. Storey, R. D. Muller, and L. A. Gahagan (2002), Kerguelen hotspot magma output since 130 Ma, *J. Petrol.*, *43*, 1121–1139.

Contreras-Reyes, E., I. Grevemeyer, A. B. Watts, L. Planert, E. R. Flueh, and C. Peirce (2010), Crustal intrusion beneath the Louisville hotspot track, *Earth Planet. Sci. Lett.*, *289*, 323–333, doi:10.1016/j.epsl.2009.11.020.

Couch, R., and R. Whitsett (1981), *Structures of the Nazca Ridge and the Continental Shelf and Slope of Southern Peru*, *Mem. Geol. Soc. Am.*, pp. 154.

Davies, G. (1988), Ocean bathymetry and mantle convection: 1. Large-scale flow and hotspots, *J. Geophys. Res.*, *93*, 10,467–10,480, doi:10.1029/JB093iB09p10467.

Detrick, R. S., and A. B. Watts (1979), An analysis of isostasy in the world's oceans: 3. Aseismic ridges, *J. Geophys. Res.*, *84*, 3637–3653, doi:10.1029/JB084iB07p03637.

Dingle, R. V., and E. Simpson (1977), The Walvis ridge: A review, in *Geodynamics, Progress and Prospects*, *Spec. Publ.*, vol. 5, AGU, Washington, D. C.

Duncan, R. (2002), A time frame for construction of the Kerguelen Plateau and Broken Ridge, *J. Petrol.*, *43*(n7), 1109–1119.

Farnetani, C., M. A. Richards, and M. Ghiorso (1996), Petrological models of magma evolution and deep crustal structure beneath hotspots and flood basalt provinces, *Earth Planet. Sci. Lett.*, *143*, 81–94.

Feighner, M., and M. A. Richards (1994), Lithospheric structure and compensation mechanisms of the Galápagos Archipelago, *J. Geophys. Res.*, *99*, 6711–6729, doi:10.1029/93JB03360.

Feighner, M., and M. A. Richards (1995), The fluid dynamics of plume-ridge and plume-plate interactions: An experimental investigation, *Earth Planet. Sci. Lett.*, *129*(1–4), 171–182.

Foulger, G. (2002), Plumes, or plate tectonic processes?. [Available at https://community.dur.ac.uk/g.r.foulger/Offprints/Astron-Geo.pdf.]

Frey, F., et al. (2000), Origin and evolution of a submarine large igneous province: The Kerguelen Plateau and Broken Ridge, southern Indian Ocean, *Earth Planet. Sci. Lett.*, *176*, 73–89.

Geli, L., D. Aslanian, J. L. Olivet, I. Vlastelic, L. Dosso, H. Guillou, and H. Bougault (1998), Location of Louisville hotspot and origin of Hollister Ridge: Geophysical constraints, *Earth Planet. Sci. Lett.*, *194*, 31–40.

Gibson, S., R. N. Thompson, J. A. Day, S. E. Humphris, and A. P. Dickin (2005), Melt-generation processes associated with the Tristan mantle plume: Constraints on the origin of EM-1, *Earth Planet. Sci. Lett.*, *237*, 744–767.

Google Earth Software (version 7.1.8.3036), Plus gobal sattelite-derived gravity anomaly. [Available at http://topex.ucsd.edu/grav_outreach/], plus 'Age of the Lithosphere for Google Earth'. [Available at http://nachon.free.fr/GE/Welcome.html.]

Goslin, J., and J. Sibuet (1975), Geophysical study of the easternmost Walvis Ridge, South Atlantic: Deep structure, *Geol. Soc. Am. Bull.*, *86*, 1713–1724.

Hampel, A., N. Kukowski, J. Bialas, C. Huebscher, and R. Heinbockel (2004), Ridge subduction at an erosive margin: The collision zone of the Nazca Ridge in southern Peru, *J. Geophys. Res.*, *109*, B02101, doi:10.1029/2003JB002593.

Hieronymus, F., and D. Bercovici (2001), A theoretical model of hotspot volcanism: Control on volcanic spacing and patterns via magma dynamics and lithospheric stresses, *J. Geophys. Res.*, *106*, 683–702, doi:10.1029/2000JB900355.

Hillier, J. K. (2007), Pacific seamount volcanism in space and time, *Geophys. J. Int.*, *168*, 877–889.

King, S. D., and C. Adam (2014), Hotspot swells revisited, *Phys. Earth Planet. Int.*, *235*, 66–83, doi:10.1016/j.pepi.2014.07.006.

Kostoglodov, V., M. G. Kogan, and E. Magnitskaya (1981), Isostasy of the southern Mid-Atlantic Ridge: Long-wavelength and short-wavelength effects, *J. Geophys. Res.*, *86*, 7825–7841, doi:10.1029/JB086iB09p07825.

Krishna, K., Y. P. Neprochnov, D. Gopala Rao, and B. N. Grinko (2001), Crustal structure and tectonics of the Ninetyeast Ridge from seismic and gravity studies, *Tectonics*, *20*, 416–433, doi:10.1029/2001TC900004.
Kruse, S., J. Zhengrong, D. Naar, and R. Duncan (1997), Effective elastic thickness of the lithosphere along the Easter Seamount Chain, *J. Geophys. Res.*, *102*, 27,305–27,317, doi:10.1029/97JB02158.
Kumar, N. (1979), Origin of "paired" aseismic rises: Ceara and Sierra Leone rises in the equatorial, and the Rio Grande Rise and Walvis Ridge in the South Atlantic, *Mar. Geol.*, *30*(1979), 175–191.
Lonsdale, P. (1988), Geography and history of the Louisville hotspot chain in the Southwest Pacific, *J. Geophys. Res.*, *93*, 3078–3104, doi:10.1029/JB093iB04p03078.
Lyons, S., D. Sandwell, and W. Smith (2000), Three-dimensional estimation of elastic thickness under the Louisville Ridge, *J. Geophys. Res.*, *105*, 13,239–13,252, doi:10.1029/2000JB900065.
Mihalffy, P., B. Steinberger, and H. Schmeling (2008), The effect of the large-scale mantle flow field on the Iceland hotspot track, *Tectonophysics*, *447*, 5–18.
Mukhopadhyyay, M., and M. Krishna (1995), Gravity anomalies and deep structure of the Ninetyeast Ridge north of the equator, eastern Indian Ocean—A hotspot trace model, *Mar. Geophys. Res.*, *17*, 201–216.
Nurnberg, D., and D. Muller (1991), The tectonic evolution of the South Atlantic from Late Jurassic to present, *Tectonophysics*, *191*, 21–53.
O'Connor, J. M., and J. R. Duncan (1990), Evolution of the Walvis Ridge-Rio Grande rise hot spot system: Implications for African and South American plate motions over plumes, *J. Geophys. Res.*, *95*, 17,475–17,502, doi:10.1029/JB095iB11p17475.
O'Connor, J., W. Jokat, A. P. Le Roex, C. Class, J. R. Wijbrans, S. Keßling, K. F. Kuiper, and O. Nebel (2012), Hotspot trails in the South Atlantic controlled by plume and plate tectonic processes, *Nat. Geosci.*, *5*, 735–738, doi:10.1038/NGEO1583.
Orellana-Rovirosa, F., and M. A. Richards (2015), Evidence and models for lower crustal flow beneath the Galápagos platform, *Geochem. Geophys. Geosyst.*, *17*, 113–142, doi:10.1002/2015GC006136.
Phipps Morgan, J. (1997), The generation of a compositional lithosphere by mid-ocean ridge melting and its effect on subsequent off-axis hotspot upwelling and melting, *Earth Planet. Sci. Lett.*, *146*, 213–232.
Pilger, R., and D. Handshumacher (1981), The fixed-hotspot hypothesis and origin of the Easter-Sala y Gomez-Nazca trace, *Geol. Soc. Am. Bull.*, *92*, 437–446.
Ribe, N. M., and U. R. Christensen (1999), The dynamical origin of the Hawaiian volcanism, *Earth Planet. Sci. Lett.*, *171*, 517–531.
Ribe, N. M., and W. L. Delattre (1998), The dynamics of plume-ridge interaction III. The effects of ridge migration, *Geophys. J. Int.*, *133*, 511–518.
Richards, M., E. Contreras-Reyes, C. Lithgow-Bertelloni, M. Ghiorso, and L. Stixrude (2013), Petrological interpretation of deep crustal intrusive bodies beneath oceanic hotspot provinces, *Geochem. Geophys. Geosyst.*, *14*, 604–619, doi:10.1029/2012GC004448.
Royer, J.-Y., J. W. Peirce, and J. K. Weissel (1991), Tectonic constraints on the hot-spot formation of Ninetyeast Ridge, in *Proceedings ODP Science Results*, vol. 121, edited by J. K. Weissel et al., pp. 763–776, Ocean Drilling Program, College Station, Tex.
Sleep, N. (1990), Hotspots and mantle plumes: Some phenomenology, *J. Geophys. Res.*, *95*, 6715–6736, doi:10.1029/JB095iB05p06715.
Sleep, N. (1996), Lateral flow of hot plume material ponded at sublithospheric depths, *J. Geophys. Res.*, *101*, 28,065–28,083, doi:10.1029/96JB02463.
Sleep, N. (2002), Ridge-crossing mantle plumes and gaps in tracks, *Geochem. Geophys. Geosyst.*, *3*(12), 8505, doi:10.1029/2001GC000290.
Sreejith, K. M., and K. S. Krishna (2013), Spatial variations in isostatic compensation mechanisms of the Ninetyeast Ridge and their tectonic significance, *J. Geophys. Res. Solid Earth*, *118*, 5165–5184, doi:10.1002/jgrb.50383.
Sreejith, K. M., and K. S. Krishna (2015), Magma production rate along the Ninetyeast Ridge and its relationship to Indian plate motion and Kerguelen hot spot activity, *Geophys. Res. Lett.*, *42*, 1105–1112, doi:10.1002/2014GL062993.
Tiwari, V. M., I. Grevemeyer, B. Singh, and J. Phipps Morgan (2007), Variation of effective elastic thickness and melt production along the Deccan–Reunion hotspot track, *Earth Planet. Sci. Lett.*, *264*, 9–21.
Torsvik, T., H. Amundsen, E. Hartz, F. Corfu, N. Kusznir, C. Gaina, P. Doubrovine, B. Steinberger, L. Ashwal, and B. Jamtveit (2013), A Precambrian microcontinent in the Indian Ocean, *Nat. Geosci.*, *6*, 223–227, doi:10.1038/ngeo1736.
Torsvik, T., et al. (2015), Continental crust beneath southeast Iceland. [Available at http://www.pnas.org/lookup/suppl/doi:10.1073/pnas.1423099112/-/DCSupplemental.]
Turcotte, D., and G. Shubert (2002), *Geodynamics*, 2nd ed., Cambridge Univ. Press, New York.
Watts, A. B. (1978), An analysis of isostasy on the world's oceans, 1. Hawaiian-Emperor seamount chain, *J. Geophys. Res.*, *83*, 5989–6004, doi:10.1029/JB083iB12p05989.
Watts, A. B. (2001), *Isostasy and Flexure of the Lithosphere*, Cambridge Univ. Press, Cambridge.
Watts, A. B., and U.S. Ten Brink (1989), Crustal structure, flexure, and subsidence history of the Hawaiian Islands, *J. Geophys. Res.*, *94*, 10,473–10,500, doi:10.1029/JB094iB08p10473.
Werner, R., K. Hoernle, U. Barckhause, and F. Hauff (2003), Geodynamic evolution of the Galápagos hotspot system (Central East Pacific) over the past 20 m.y.: Constraints from morphology, geochemistry, and magnetic anomalies, *Geochem. Geophys. Geosys.*, *4*, 1108, doi:10.1029/2003GC000576.
Wessel, P. (2016), Regional–residual separation of bathymetry and revised estimates of Hawaii plume flux, *Geophys. J. Int.*, *204*, 932–947, doi:10.1093/gji/ggv472.
Wessel, P., and L. W. Kroenke (2009), Observations of geometry and ages constrain relative motion of Hawaii and Louisville plumes, *Earth Planet. Sci. Lett.*, *284*, 467–472.
Wilder, D. (2003), Relative motion history of the Pacific-Nazca (Farallon) plates since 30 Ma ago, MS thesis, College of Mar. Sci., Univ. Florida, Fla.